# Stability Control and Trajectory Optimization of Tail-Sitter VTOL UAV Takeoff / Landing Incorporating Bionic Technology

QI Hao[1,2], LI Qingyang[1,3], WU Jiayue[1,4], PENG Yiming[1,2], NIE Hong[1,2], WEI Xiaohui[1,2*]

1. State Key Laboratory of Mechanics and Control for Aerospace Structures, Nanjing University of Aeronautics and Astronautics, Nanjing 210016, P.R. China;
2. Key Laboratory of Fundamental Science for National Defense Advanced Design Technology of Flight Vehicle, Nanjing University of Aeronautics and Astronautics, Nanjing 210016, P.R. China;
3. China Aviation Power Plant Research Institute, Zhuzhou 412002, P.R. China;
4. School of Automation Science and Electrical Engineering, Beihang University, Beijing 100191, P.R. China

**Abstract:** The tail-sitter vertical takeoff / landing (VTOL) unmanned aerial vehicle (UAV) exhibits poor stability and limited compatibility with traditional landing gears. To address the aforementioned issues, a novel landing gear incorporating free-tail technology is proposed. The landing gear adopts a tandem multi-stage structure, which can ensure the length of the tail force arm in cruise condition while lowering the fuselage altitude. Furthermore, the dynamic landing process is regulated through the employment of virtual centroid force distribution techniques, streamlining the control process and facilitating seamless trajectory optimization during mode transition. Based on the single-point dataset of the cat center point, a neural network is used to train the landing gear control, which makes the landing gear adaptive takeoff and landing speed and accuracy effectively improved. Subsequently, multi-objective optimization and similarity conversion are executed in conjunction with parameter requirements of different modes of the UAV, effectively enhancing landing adaptability and stability of the tail-sitter VTOL UAV.

**Key words:** unmanned aerial vehicle (UAV); vertical takeoff / landing (VTOL); takeoff / landing technology; stability control; bionic technology

## 0　Introduction

The tail-sitter vertical takeoff / landing (VTOL) unmanned aerial vehicle (UAV), which is designed to takeoff in a tail-sitter position and transition to level flight once it reaches a certain altitude, is the subject of this study. During landing, the UAV ascends and tilts its nose upward before reducing thrust for a vertical descent. The thrust direction of the UAV is fixed along the longitudinal axis of the aircraft, allowing it to rotate synchronously with the UAV when changing direction[1]. However, due to its fixed-wing structure and upright fuselage, the tail-sitter VTOL UAV exhibits poor stability during takeoff / landing, resulting in a high center of gravity and a large windward area. This limitation hinders its widespread usage.

The takeoff / landing stability of helicopters is comparable to that of tail-sitter VTOL UAVs. Kubo et al. and De Wagter et al.[2-3] delved into the causes and preventive measures of dynamic rollover in helicopters. Upon making contact with the ground, a novel pivot point emerges, such as a skid or tire. Dynamic rollover transpires when the flight controls fail to impede the progression of lateral an-

gular velocity around this pivot point. In order to guarantee secure takeoff / landing, the gradient of the landing surface should be restricted to 6°—15°[4]. In comparison to helicopters, the landing gear of most tail-sitter VTOL UAVs is comparatively narrower, and their pitch control effectors are less effective than those of helicopters, which utilize thrust vector control. The pitch control of google project wing is accomplished through differential thrust generated by propellers installed on both the upper and lower sides of the wing. Some tail-sitters also employ aerodynamic effectors immersed in propeller slipstream for balance or use rotating swashplates for blade pitch control[5]. As a result, the takeoff / landing techniques of tail-sitter VTOL UAVs are more critical and intricate.

Currently, most tail-sitter VTOL test prototypes and civilian models with fixed landing gear are limited to a single function and role. Relying on the bending deformation of their own structure, these models absorb and dissipate vertical energy during the landing process. Only a few models, such as the "Sky Eye" and "Tern"[6], use wheeled or skid type landing gear that are effective during skate takeoff / landing. These models rely on the airframe structure during vertical takeoff / landing. The "Spirit Stilts" uses a curved skid on the abdomen to achieve attitude change from flat to vertical takeoff / landing before the fuselage leaves the ground. This design allows for vertical landing at any angle but requires special attention in terms of power vector and design. In order to improve energy release buffering capacity, well-known tail-sitter VTOL UAVs such as "XFY-1" "Sky-Tote" "Golden-Eye", and "X-Plane" have added strut type buffers at the bottom[7-10]. However, problems persist with single function fixed landing gear, weak impact resistance, poor takeoff/landing stability, and susceptibility to rebound and rollover. Even the "THU-1600"[11] of Tsinghua University proposed a controlled forward landing scheme. This involves giving the body a forward tilt angle when the UAV lands vertically. The landing gear touches the ground, and the strutted landing leg at the bottom absorbs the impact. The body then uses the tipping trend to ensure safe landing with the cushioning device on the belly.

With the emergence of innovative landing devic-

es, VTOL UAVs have conducted research on new techniques for takeoff and landing. For example, the "Flexrotor"[12] tail-sitter VTOL UAV from Aerovel features a one-piece flexible landing gear structure that resolves the conflict between retaining the tail and fuselage height. However, the landing dynamics of its elastic structure have not been extensively studied. Additionally, the fixed elastic parameters of its landing gear may cause rebound and instability issues when dealing with varying landing speeds and attitudes. In 2015, DARPA developed an adaptive landing system that arranges four mechanical feet symmetrically on either side of the fuselage can allow helicopters to land on rough ground, steps, and 20° slopes. From 2013 to 2021, Manivannan et al. [13] have introduced adaptive landing legs for UAVs. These four-legged legs feature a two-stage articulated structure that enables adaptive takeoff and landing on irregular terrains. Despite their adaptability, the storage of these legs presents challenges as they protrude significantly after folding and storing on the helicopter fuselage's bottom side, increasing the aircraft's aerodynamic resistance during high-speed cruising. As a result, future efforts will focus more on improving the cable of landing gear, motor drive structure and feedback response rather than storage functionality. In 2022, Stanford University developed a bionic landing leg called "SNAG"[14]. This innovative leg can lock onto various surfaces, including perchable branches, dropped spheres, or skeletons. However, like Georgia Tech quadruped adaptive landing gear, the "SNAG" also features a box-shaped structure that protrudes from the bottom of the fuselage after retraction, causing potential aerodynamic drawbacks during flight.

Therefore, the aforementioned solutions have yielded noteworthy enhancements in the local performance of fixed landing gear. They still exhibit certain limitations[15-17], particularly with regards to landing constraints, which have emerged as a crucial technological bottleneck hindering the advancement of tail-sitter VTOL UAV.

# 1 Modeling of Landing Gear Kinematic and Dynamics

In this study, the free tail is utilized and a bio-

mimetic approach is used to mimic the structure of the free tail technology, capture its movements and collect the relevant data, so the first step is to model the dynamics and kinematics of the landing gear.

　　To enhance the adaptability of landing gear to the dual mode of VTOL/cruise for tail-sitter VTOL UAVs, this study proposes a design approach that integrates the landing gear structure with the overall layout optimization. The concept of structural functional integration design is employed, aiming to improve the performance and efficiency of tail-sitter VTOL UAVs. As illustrated in Fig.1 and Fig.2, the landing gear comprises tail support and support strut, which form a foldable two-section structure. They are installed symmetrically on both sides of the fuselage, connected by a driving mechanism that enables the tail support and support strut to open and close. This mechanism allows the landing gear to transition between modes and adjust its attitude for adaptive support during landing. The proposed design approach not only enhances the landing gear's stability and adaptability but also advances the overall performance of tail-sitter VTOL UAVs.



Fig.1　Conceptual diagram of the tail-sitter VTOL UAV incorporating free-tail in cruise state



Fig.2　Conceptual diagram of the tail-sitter VTOL UAV incorporating free-tail in takeoff / landing state

## 1. 1　Kinematic modeling of the tail-sitter VTOL UAV incorporating free-tail

　　During the takeoff / landing process of a tail-sitter VTOL UAV, only the motion characteristics on the central plane are typically studied, with little consideration given to the coronal plane. Additionally, due to the uniform motion model of the front and rear landing gear during takeoff / landing, the tail-sitter VTOL UAV can be viewed as a two-dimensional planar multi-rigid body system. The takeoff / landing process can be divided into three phases: Takeoff, approach, and landing, based on whether the landing gear is in contact with the ground.

　　Establish a body coordinate system $\{O_b\}$ at the geometric center of the fuselage, with the forward direction as the positive direction of the $x$-axis and the upward direction as the positive direction of the $z$-axis. Number the landing gears clockwise as 1, 2, 3, 4. Establish coordinate systems $\{O_{ih}\}(i=1,2,3,4)$ at the connection joints between each landing gear and the fuselage, with the positive direction of the $x$-axis of $\{O_{ih}\}$ as the downward direction and the positive direction of the $z$-axis as the forward direction. Similarly, establish coordinate systems $\{O_{ik}\}$ at the joints of the support strut and tail support, with the bottom of the landing gear as the origin of the coordinate system $\{O_{it}\}$. From this, the transformation matrix $N$ from the body coordinate system to the coordinate system of the connection joint between the landing gear and the fuselage can be obtained. Taking the assumption that the left side is the first side to touch the ground as an example, assume that the function of the trajectory of the bottom of the landing gear in the body coordinate system is $z=f(x,y)$. From the coordinates $P$ of the bottom of the landing gear in the body coordinate system, the coordinates $P_0$ of the bottom of the landing gear in the coordinate system of the connection joint between the landing gear and the fuselage can be obtained. From this, the rotation angles of the tail support and the support strut can be solved inversely.

$$N=\begin{bmatrix} 1 & 0 & 0 & \dfrac{\mathrm{dis}_x}{2} \\ 0 & 0 & -1 & \dfrac{\mathrm{dis}_y}{2} \\ 0 & 1 & 0 & 0 \\ 0 & 0 & 0 & 1 \end{bmatrix} \tag{1}$$

$$P_0=\begin{bmatrix} x_0 & y_0 & z_0 & 1 \end{bmatrix}^{\mathrm{T}}=N*P \tag{2}$$

where $\mathrm{dis}_x$ is the distance between the landing gears

on the same side of the fuselage and $dis_y$ the distance between the landing gears on both sides of the fuselage.

### 1.1.1 Takeoff phase

During the takeoff phase, it is imperative to maintain stability by ensuring adequate friction between the landing gear and the ground, thereby minimizing relative sliding during takeoff. Additionally, the connection joint between the landing gear and the fuselage must meet specific criteria with respect to the coordinates of the landing gear base.

(1) The initial height of the fuselage is $y_0$, the horizontal displacement is 0 m, the height of the fuselage before takeoff is $y_1$, and the horizontal displacement is $x_1$. (2) The initial velocity is 0 m/s, and the velocity before leaving the ground is $v_1$. (3) The initial acceleration is 0 m/s². Before leaving the ground, the vertical acceleration is $-g$, and the horizontal acceleration is $a_{x_1}$.

During in takeoff phase, the bottom end of the landing gear is fixed in the earth coordinate system. The motion equation of the centroid of the planned tail-sitter VTOL UAV is based on the bottom end of the landing gear as a reference. Since during the takeoff phase, one side of the landing gear will inevitably leave the ground first. The structure and motion of the landing gear on the ground side are the same. Therefore, only the motion of a single landing gear needs to be considered. Assuming that centroid of the UAV is in the takeoff phase, the horizontal acceleration $a_x(t)=k_1t$ and the vertical acceleration $a_y(t)=k_2t$ ($k_1$ and $k_2$ are the constant coefficients), $R$ is the trajectory of the fuselage center of gravity. Then the horizontal displacement is $R_x(t)=1/6k_1t^3$ and the vertical displacement is $R_y(t)=1/6k_2t^3$.

Assuming the origin $O$ to be located at the bottom of the landing gear, the coordinates of the connection joint between the landing gear and the fuselage can be denoted as $B(P_X,P_Y)$, and the coordinate system can be established as illustrated in Fig.3.

The length of the landing gear at the end connected to the fuselage is $L_2$, the length of the landing gear at the touchdown end is $L_1$, the angle with
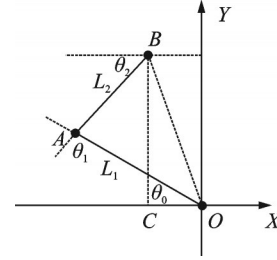


Fig.3   Coordinate system for landing gear joints during take-off

the ground is $\theta_0$, and the complementary angle of the angle between the two landing gears is $\theta_1$.

The transformation matrix of the connection joint between the landing gear and the fuselage in the base coordinate is as follows

$$N=$$
$$\begin{bmatrix} \cos(\theta_0+\theta_1) & -\sin(\theta_0+\theta_1) & 0 & L_1\cos(\theta_0+\theta_1)+L_2\cos\theta_0 \\ \sin(\theta_0+\theta_1) & \cos(\theta_0+\theta_1) & 0 & L_1\sin(\theta_0+\theta_1)+L_2\sin\theta_0 \\ 0 & 0 & 0 & 0 \\ 0 & 0 & 0 & 1 \end{bmatrix}$$

(3)

The analysis of the takeoff phase through inverse kinematics is executed utilizing the geometric analytic method, resulting in the derivation of the joint rotation angle function

$$\begin{cases} \theta_1=-\arccos\left[\dfrac{L_1^2+L_2^2-(P_X^2+P_Y^2)}{2L_1L_2}\right] \\ \theta_0=\arctan\left(-\dfrac{P_Y}{P_X}\right)-\arccos\left[\dfrac{L_1^2-L_2^2+(P_X^2+P_Y^2)}{2L_1\sqrt{P_X^2+P_Y^2}}\right] \end{cases}$$

(4)

### 1.1.2 Approach phase

In addition to the change in phase, some of the angles are partially different in expression due to the transition between obtuse and acute angles that occurs. The transformation matrix of the connection joint between the landing gear and the fuselage in the base coordinate is as follows

$$N=$$
$$\begin{bmatrix} \cos(\theta_1+\theta_2) & -\sin(\theta_1+\theta_2) & 0 & L_2\cos(\theta_1+\theta_2)+L_1\cos\theta_1 \\ \sin(\theta_1+\theta_2) & \cos(\theta_1+\theta_2) & 0 & L_2\sin(\theta_1+\theta_2)+L_1\sin\theta_1 \\ 0 & 0 & 0 & 0 \\ 0 & 0 & 0 & 1 \end{bmatrix}$$

(5)

The angular driving function for the approach air process is obtained

$$\begin{cases} \theta_1 = \pi - \arccos\left[\dfrac{L_1^2 + L_2^2 - (P_X^2 + P_Y^2)}{2L_1 L_2}\right] \\ \theta_2 = \arctan\dfrac{P_Y}{P_X} - \arccos\left[\dfrac{L_1^2 - L_2^2 + (P_X^2 + P_Y^2)}{2L_1\sqrt{P_X^2 + P_Y^2}}\right] \end{cases} \quad (6)$$

During takeoff, the elevation of landing gear must be adjusted to conform to the ground environment and clear any obstructions. The trajectory of the landing gear bottom is adjusted using a sine function curve and a second order polynomial, based on the maximum height of obstacles that can be cleared, denoted as $H$. Furthermore, a second-order polynomial can be used to fit the landing gear bottom trajectory to the transverse coordinate $x$ and longitudinal coordinate $y$.

$$\begin{cases} x = \dfrac{R}{T}t & 0 < t < T \\ y = \begin{cases} H\sin\left(\dfrac{\pi}{T}t\right) & 0 < t < \dfrac{T}{2} \\ \dfrac{4H}{T^2}(t - T)^2 & \dfrac{T}{2} < t < T \end{cases} \end{cases} \quad (7)$$

### 1.1.3　Landing phase

Upon touchdown, the motor torque drives generate an opposing force that counteracts the inertia of the fuselage. This force causes a reduction in the velocity of the tail-sitter VTOL UAV until it reaches a velocity of 0, marking the conclusion of the landing phase. Viewed in contrast to the takeoff phase, the landing phase can be considered its inverse. The center of mass displacement curve during the landing phase may be represented by $R = vt - 16kt^3$.

### 1.2　Dynamics modeling of the tail-sitter VTOL UAV incorporating free-tail

This study employs Lagrange's and D'Alembert's principles to analyze the dynamics of the tail-sitter VTOL UAV. The motion planning process is employed to determine the driving moments for each joint during the takeoff process, resulting in a comprehensive understanding of the driving force function of the motor, thereby ensuring seamless operation.

The mechanical structures of the tail-sitter VTOL UAV are assumed to be rigid with no allowance made for flexible deformation, while ignoring

the relative friction between joints and errors in the equipping process of the physical prototype. Given the simplicity of the takeoff phase dynamics, this study restricts its focus to the aerial approach and landing phase. To facilitate further analysis, motion coordinates are established at the outset.

$$\begin{cases} (X_1, Y_1) = (-P_1\cos\theta_1, -P_1\sin\theta_1) \\ (X_2, Y_2) = (-L_1\cos\theta_1 - P_2\cos(\theta_1 + \theta_2), \\ \quad -L_1\sin\theta_1 - P_2\sin(\theta_1 + \theta_2)) \end{cases} \quad (8)$$

where $\theta_1$ represents the swing angle of the tail brace, $\theta_2$ the swing angle of the support bar, $P_1$ the distance from the centroid of the tail brace to the point where it connects with the fuselage, and $P_2$ the distance from the center of mass of the support bar to the point where it connects with the tail brace. Additionally, $(X_1, Y_1)$ represents the coordinates of the centroid of the tail brace, while $(X_2, Y_2)$ represents the coordinates of the center of mass of the support bar. At this juncture, the kinetic energy $E_k$ and the potential energy $E_p$ can be calculated as follows

$$\begin{cases} E_{k1} = \dfrac{1}{2}m_1 v_1^2 = \dfrac{1}{2}m_1(\dot{X}_1^2 + \dot{Y}_1^2) = \dfrac{1}{2}m_1 P_1^2 \dot{\theta}_1^2 \\ E_{k2} = \dfrac{1}{2}m_2 v_2^2 = \dfrac{1}{2}m_2(\dot{x}_2^2 + \dot{y}_2^2) = \\ \quad \dfrac{1}{2}m_2 L_1^2 \dot{\theta}_1^2 + \dfrac{1}{2}m_2 P_2^2(\dot{\theta}_1 + \dot{\theta}_2)^2 + \\ \quad m_2 L_1 P_2\cos\theta_2(\dot{\theta}_1^2 + \dot{\theta}_1\dot{\theta}_2) \end{cases} \quad (9)$$

$$\begin{cases} E_{p1} = m_1 g P_1(1 - \sin\theta_1) \\ E_{p2} = m_2 g L_1(1 - \sin\theta_1) + m_2 g P_2(1 - \sin(\theta_1 + \theta_2)) \end{cases}$$
$$(10)$$

where $E_{k1}$ is the kinetic energy of tail brace, $E_{k2}$ the kinetic energy of support bar, $E_{p1}$ the potential energy of tail brace, $E_{p2}$ the potential energy of support bar. Get the Lagrange function: $L = E_k - E_p$.

During landing, the inertia of the airframe necessitates a force in the opposite direction. Assuming that there is no relative sliding between the bottom end of the landing gear and the ground, and the ground provides static friction to the tail-sitter VTOL UAV, where $M_1$ represents the driving moment of the joints that connect the landing gear to the fuselage, $M_2$ embodies the driving moment of the joints that connect the tail support to the support strut. We can utilize D'Alembert's principle to ana-

lyze the equilibrium of the landing gear

$$
\begin{cases}
M_1 = F_y L_1 \cos \theta_1 - F_x L_1 \sin \theta_1 \\
M_2 = F_y L_2 \sin\left(\theta_1 + \theta_2 - \dfrac{\pi}{2}\right) + F_x L_2 \sin(\theta_1 + \theta_2)
\end{cases}
$$

$$(11)$$

To prevent rollover, it is essential to maintain the moment at the centroid of the tail-sitter VTOL UAV body as close to 0 as possible, thus

$$
\begin{cases}
F_{y1} + F_{y4} = \dfrac{F_y}{2} \\
F_{x1} + F_{x4} = \dfrac{F_x}{2} \\
F_y \Delta L - F_x h + 2\left(F_{y4} - F_{y1}\right) L_Q = \tau_{-z} = 0
\end{cases}
$$

$$(12)$$

where the horizontal and vertical forces at the bottom of the $i$th landing gear are represented by $F_{xi}$ and $F_{yi}$, respectively; $F_x$ and $F_y$ denote the horizontal and vertical forces acting on the center of mass of the tail-sitter VTOL UAV fuselage. $\Delta L$ is the difference of $L$, $h$ the vertical distance from the end of the support bar to the point where the tail brace joins the fuselage, $L_Q$ the horizontal distance between the center of mass and the hip joint, and $\tau_{-z}$ the moment at the center of mass.

## 2 Bionic Simplified Data Acquisition and Training

Since the proposal of the zero moment point (ZMP) theory[18], its related methods have been frequently used for determining robot stability. The advantage of this method is that it fully utilizes mathematical models to carefully analyze and describe the kinematic constraints and dynamic stability conditions. However, there exists a significant gap between the coordination of trajectories of each joint in robots and that of natural organisms, particularly in transient and complex dynamic tasks. The analytical form of the equations of motion is difficult to establish and solve, resulting in poor maneuverability.

To enhance the intelligence of robots and achieve more complex and diversified tasks, bionic technology has gained attention[19-21]. By utilizing the natural and smooth movement transitions and energy optimization of living creatures, such as cats, it is possible to not only fully utilize the morphological advantages of bionic robots but also improve their behavior and movement.

In this study, we have selected the cat as the bionic target due to its excellent landing performance. Building upon the experimental findings of other researchers on the biological structure of cats and their typical landing states[22-23], as illustrated in Fig.4, traditional data conversion methods are commonly used to divide the movement data of cats into multiple key nodes to obtain trajectory coordinates in different movement processes. However, this approach is limited in scenarios requiring high data reconstruction accuracy and small loss values.



(a) Biological structure and experimental data of cats

(b) Image processing of experimental data

(c) Data extraction for joint nodes
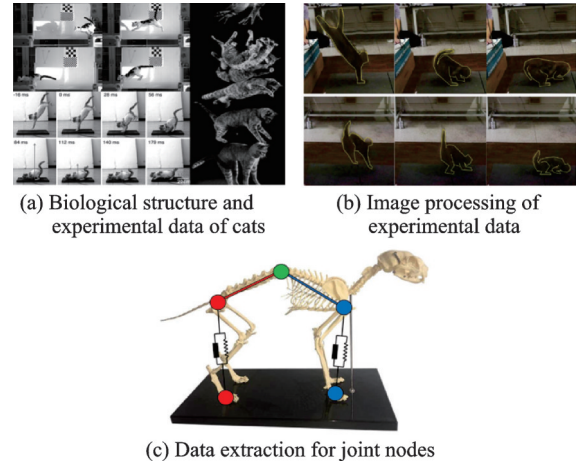
Fig.4   Schematic diagram of feature map transformation

Therefore, to simplify the control of the landing gear, this study adopts a virtual centroid force system allocation approach. This allocation is simplified into a single rigid body virtual centroid force system with rigid body motion. When controlling the motion of this rigid body, the virtual centroid force system is first calculated based on the relationship between the target position and the current position. Then, the virtual centroid force system is decomposed into four actual control forces. The allocation of the virtual centroid force system is a dynamic process. When the virtual centroid force system remains unchanged, the force allocation scheme depends only on the current attitude. When the attitude remains unchanged, the force allocation scheme depends only on the virtual centroid force system. However, in reality, both the virtual center

of mass force system and the tail-sitter VTOL UAV airframe attitude are variables and contain a large data space. To efficiently train neural network weights for fitting complex tasks and automatically learn sample data features from unlabeled samples, this study uses a self-supervised learning method called self-encoder.

The conventional self-encoder architecture involves remapping input data into lower-dimensional and more significant features via the encoding layer. The resulting low-dimensional data can be compressed and reconstructed using the decoding layer. The network parameters are optimized by minimizing the loss values between the reconstructed data and the input data. Once the loss values meet the task requirements, the feature outputs can be regarded as the features of the original data in the low-dimensional space. However, the conventional self-encoder is not suitable for training the center of mass force system assignment task. Therefore, it needs to be improved. As shown in Fig.5, the assignment of the single rigid body center of mass force system can be regarded as the remapping of the 6-dimensional center of mass force system into the high-dimensional (12-dimensional) space. This remapping needs to meet the equivalence requirements: The single rigid body center of mass, as the simplification center, should be completely equivalent to the simplified center of mass force system and the target cent of mass force system through the spatial arbitrary force system simplification principle of the 12-dimensional force. Here, the vector $U_c$ denotes the target center of mass force system, and the vector $U_6$ denotes the simpli-

fied center of mass force system obtained by simplifying the 12-dimensional force. The vector $f_i$ denotes one of the 12-dimensional forces, $E$ the unit matrix, and $r_i$ the coordinate vector from the point of force action to the center of mass of the rigid body. The matrix $[r_i]_\times$ denotes the antisymmetric matrix of $r_i$, which is used to compute the vector fork multiplication.

$$\begin{bmatrix} E & E & E & E \\ [r_1]_\times & [r_2]_\times & [r_3]_\times & [r_4]_\times \end{bmatrix}\begin{bmatrix} f_1 \\ \vdots \\ f_{12} \end{bmatrix} = U_6 = U_c \quad (13)$$

The spatial arbitrary force system simplification process bears a striking resemblance to the self-encoder decoding process, which can be regarded as a reductionist reconstruction of the data. Consequently, an enhancement has been made to the self-encoder rather than employing the decoding network of the conventional self-encoder. The spatial arbitrary force system simplification process is now deemed the decoding process.

The affine strategy is denoted by $\pi_E$. The affine data generated by this strategy is stored in the affine dataset $D_E$. The distribution of this data conforms to

$$D_E = \left\{ (s_i, a_i)_{i=1}^N \overset{\text{i.i.d.}}{\sim} \rho_{\pi_E}(s, a) \right\} \quad (14)$$

where $s$ is the target centroid force system; $a$ is the four elements that can uniquely express the body posture of a quadrupedal robot.

$$s = \begin{bmatrix} f_x & f_y & f_z & t_x & t_y & t_z \end{bmatrix} \quad (15)$$

where $\rho_{\pi_E}(s, a)$ represents the non-normalized distribution of data generated by the affine strategy $\pi_E$; i.i.d. indicates that the data in the affine dataset $D_E$ are independently and identically distributed.

To cater to diverse scenarios, a double loop training process is devised, as illustrated in Fig.6.

During training, $n$ sets of vectors $D_{E1}$ are randomly generated as inner loop sample data using a uniform distribution. Upon reaching the designated number of iterations, the inner loop exits and $n$ new sets of vectors $D_{E2}$ are generated for further training. It is important to note that $D_{E1}$ and $D_{E2}$ are independent of each other.
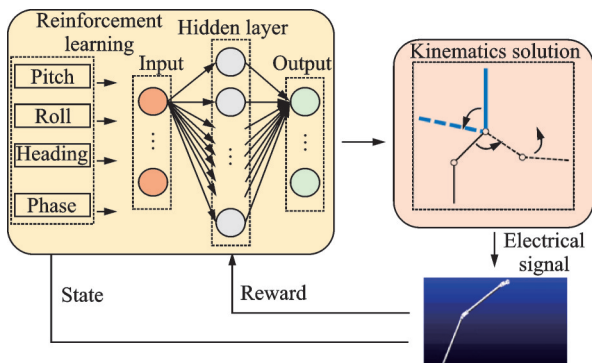


Fig.5    Simplified self-encoder structure for force systems
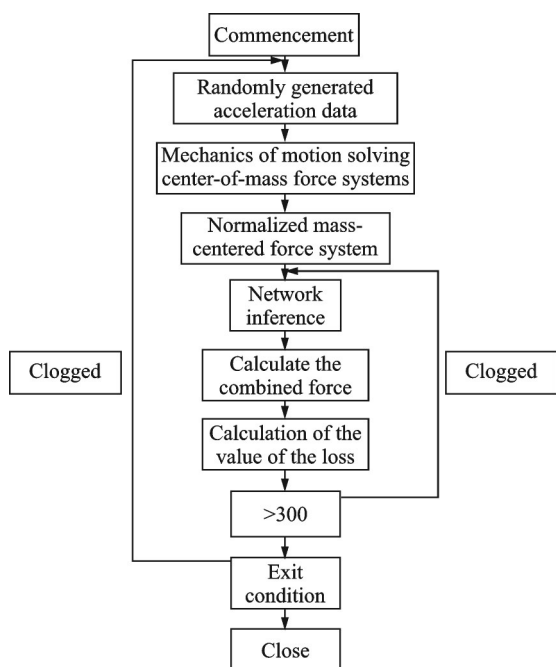
Fig.6  Internal and external dual cycle training process

After the dataset is transformed by the above bionic training and target parameter homogenization, the landing gear motion information in the takeoff / landing phase is shown in Fig.7 and Fig.8.
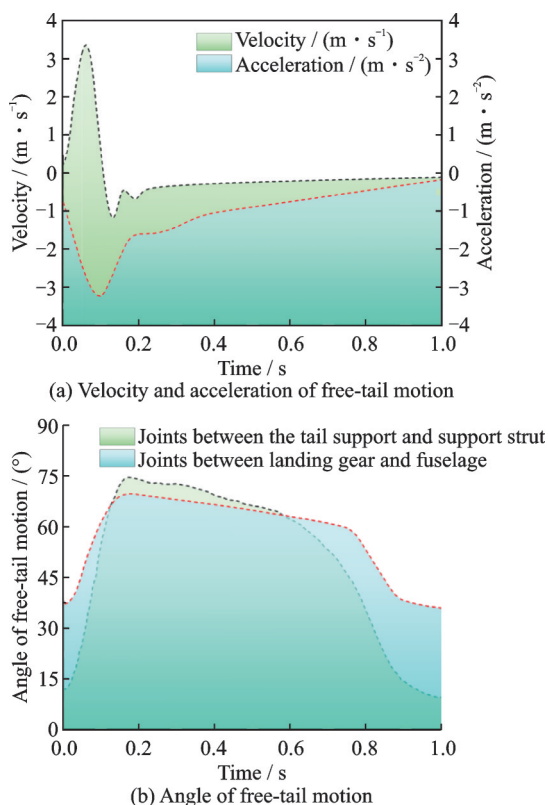


Fig.7  Landing gear movement information during the post-training takeoff phase
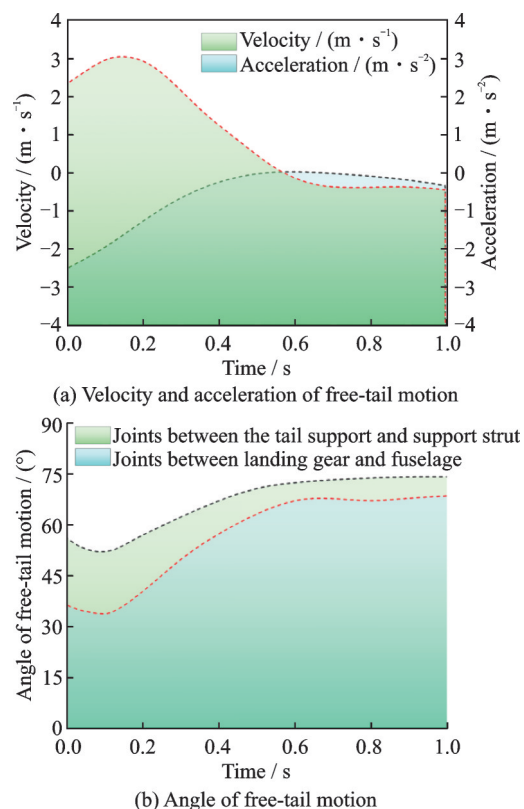


Fig.8  Landing gear motion information for post-training landing phase

# 3  Optimization of Free-Tail Parameters

The landing gear based on free-tail technology, which serves as both the structural body and the tail support of the free-tail wing. The structural parameters of this landing gear are inherently linked to the overall layout of the UAV. Consequently, this study investigates the aerodynamic interference caused by the double tail support layout under cruise conditions by considering the finite wingspan three-dimensional effect and altering the structural length of the landing gear. The pattern of aerodynamic disturbance during cruising condition is analyzed by manipulating the length of the landing gear.

To better understand the aerodynamic interaction between the rotor propeller, landing gear, and free-tail, particularly the impact of varying landing gear lengths, this study delves into the relationship between these components during cruise conditions. As depicted in Fig.9, alongside the corresponding calculation grid, it is observed that when the length of the landing gear is increased by two-thirds and

(a) Original size　(b) Lengthened by 2/3 (c) Lengthened by 3/4
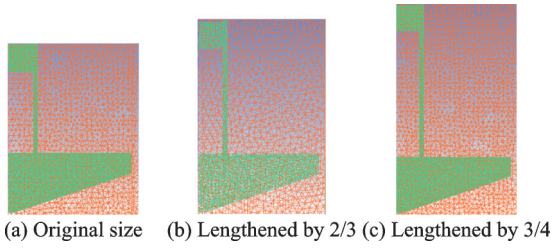
Fig.9　Position relationship and mesh of landing gear/wing in cruise state

three-quarters from Figs.9(b,c). While keeping the size of the rotating area intact, the influence of the circumferential slip interface location on the calculation results is minimized. It is recommended to position the slip interface between the rotor and stationary parts near the rotor 1/8 to 1/4 to mitigate this impact. This is because if the slip interface is positioned closer to the rotor, the rotation of the rotor will have a smaller effect on the fluid surrounding the rotor compared to if it were closer to stationary parts. However, if it were positioned closer to stationary parts, it would have a greater impact on the fluid. In light of these considerations, this study chooses a slip interface location of around 1/5, taking into account the unique characteristics of the model itself.

To mitigate the impact of the grid on the calculation results, a rigorous grid independence study is conducted prior to the analysis. Four sets of computational grids are established for the model, each with distinct grid resolutions: 70 0000, 2.1 million, 4.2 million, and 8.4 million, respectively. As illustrated in Fig.10, it is found that when the grid resolution exceeds 4 million, the calculated values of the

propeller pull coefficient and wing drag coefficient display smoother trends and exhibit less variability. This verifies that the grid resolution for the propeller/landing gear and free-tail aerodynamic interference problem is sufficient. Consequently, a computation grid consisting of 4.2 million elements was chosen for its simplicity and accuracy.

The simulation outcomes presented in Fig.11 clearly demonstrate that there is no favorable relationship between the proximity of the horizontal tail to the wing and landing gear length. When the horizontal tail is positioned too close to the wing, air converges at the rear end of the wing, leading to the formation of a vortex due to the differing flow directions of the upper and lower surfaces. The propeller slipstream exacerbates this airflow vortex, significantly increasing the instantaneous acceleration. Moreover, the influence of the propeller tip vortex persists even after bypassing the lower surface of the wing, resulting in a more irregular flow field distribution at the trailing edge of the wing. On the contrary, when the horizontal tail is positioned far away from the wing, this coupling effect is diminished, allowing the rotating slipstream to be effectively avoided. However, if the horizontal tail is positioned too far away, it could affect the center of gravity height of the tail-sitter VTOL UAV during landing, while also decreasing landing gear stiffness and increasing structural design complexity.

The length and support attitude of the landing



Fig.10　Lift curve with different number of meshes for an angle of attack of 5°
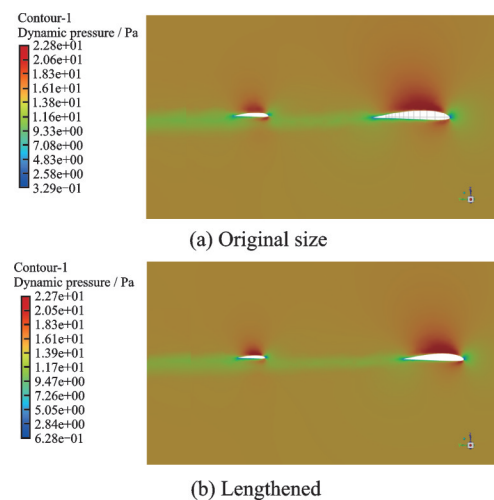


Fig.11　Landing gear length parameters on horizontal tail aerodynamic influence characteristics

gear structure are two pivotal factors that significantly influence the maximum slope of a tail-sitter VTOL UAV during landing, in addition to aerodynamic effects. By elevating the structural length, the landing gear can be provided with a larger cushion margin, while adjusting the inter-leg spacing based on changes in support attitude can enhance stability. These two factors interact with each other to affect the center of gravity altitude of the UAV. Therefore, it is crucial to conduct a static analysis on various landing gear structural lengths and support attitudes to comprehend their impact patterns.

This study employs the 1/3 times landing gear length parameter obtained from bionic biostructure as the interval to delineate the influence law of landing gear length and spacing parameters on the maximum landing slope, as illustrated in Fig.12. It can be seen that the longer the landing gear length and the larger the spacing parameter, the larger the maximum landing slope of the tail-seat VTOL UAV.
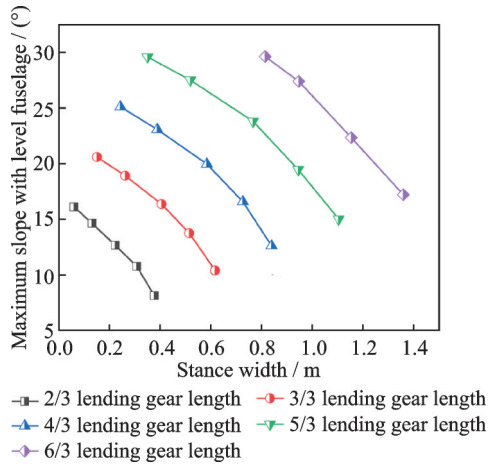


Fig.12 Influence of landing gear length and spacing parameters on the maximum landing slope

Considering the fact that the length of the landing gear has a significant impact on both the aerodynamic efficiency and landing stability of the tail-sitter VTOL UAV, necessitating its inclusion as a crucial element in the multi-objective optimization process.

The objective function begins by maximizing the efficiency of tail-sitter VTOL UAV cruise maneuvers

$$\max f_1(x) = C_{mH} \tag{16}$$

where tail wing maneuvering efficiency $C_{mH} =$

$k_q C_{LaH}((1 - \varepsilon_a)\alpha + \delta_H)\dfrac{S_H l_H}{S c_A}$, here $S_H$ is the area of the horizontal tail, $l_H$ the length of the tail force arm, $C_{LaH}$ the slope of the horizontal tail lift line, $\varepsilon_a$ the downwash at the horizontal tail, and $k_q$ the velocity retardation coefficient at the horizontal tail.

The objective function is secondly to make the tail-sitter VTOL UAV landing stability optimal. When the absolute value of the eigenvalue $\gamma$ of $A^z$ is greater than or equal to 1, the solution for the tail-sitter VTOL UAV becomes unstable.

Therefore, minimize the target $f_2(x)$.

$$\min f_2(x) = A_i^z \tag{17}$$

In the landing process of the tail-sitter VTOL UAV, the Poincaré mapping point is obtained by the state of the previous moment of the touchdown collision. Based on this, the discrete time system $x_{k+1}^z = P^z(x_k^z)$ is defined as $\partial x_k^z = x_k^z - x^{z^*}$, where $x^{z^*}$ is a fixed point. So we can get the linearized model

$$\partial x_{k+1}^z = A^z \partial x_k^z + Bu \tag{18}$$

where $A^z = [A_1^z \quad A_2^z]$, and

$$A_i^z = \frac{P^z(x^{z^*} + \Delta x_i^z) - P^z(x^{z^*} - \Delta x_i^z)}{2\Delta x_i^z} \tag{19}$$

Since the optimized landing gear parameters may differ partially from the bionic structure, it is necessary to re-evaluate the similarity of the landing process in order to apply the obtained bionic data to the design of tail-sitter VTOL UAV landing maneuvers. The system similarity metric represented by $Q$, and the closer $Q$ is to 1, the higher the similarity.

The $Q_i^{H-R}(t)$ represents the similarity between the $i$-joint of the tail-sitter VTOL UAV landing gear at time $t$ and the $i$-joint of the bionic object cat. $Q^{H-R}(t)$ is the average similarity of the whole joint at time $t$, and $Q^{H-R}$ is the average similarity within a period of trajectory time $T$.

$$Q_i^{H-R}(t) = \omega\left(1 + \frac{\phi_i^R(t) - \phi_i^H(t)}{\phi_{i\text{-max}}^R - \phi_{i\text{-min}}^R}\right)^{-1} +$$

$$(1 - \omega)\left(1 + \frac{\dot{\phi}_i^R(t) - \dot{\phi}_i^H(t)}{\dot{\phi}_{i\text{-max}}^R - \dot{\phi}_{i\text{-min}}^R}\right)^{-1} \tag{20}$$

$$Q^{H-R}(t) = \frac{\sum_{i=1}^{N} Q_i^{H-R}(t)}{N} \tag{21}$$

$$Q^{H-R} = \frac{\int_0^t Q^{H-R}(t)\,\mathrm{d}t}{T} \tag{22}$$

where $\phi_i^H(t) = [\phi_1^H(t), \phi_2^H(t), \cdots, \phi_N^H(t)]^{\mathrm{T}}$ represents the joint angle of the bionic target cat at time $t$, and $N$ is the number of joints. $\phi_i^R(t) = [\phi_1^R(t), \phi_2^R(t), \cdots, \phi_N^R(t)]^{\mathrm{T}}$ represents the joint angles of the tail-sitter VTOL UAV landing gear at time $t$. $\phi_{i\text{-max}}^R$ and $\phi_{i\text{-min}}^R$ represent the maximum and minimum rotation range of the $i$-joint of the tail-sitter VTOL UAV landing gear. $\omega$ is the transformation coefficient. When $\omega$ tends to 1, it means that the action tends to be static. When $\omega$ tends to 0, it means that the action tends to be fast conversion.

Thus the combined optimization constraints are

$$\text{s.t. } l_{i\text{-min}} \leqslant l_i \leqslant l_{i\text{-max}}$$
$$\sum_{i=1}^{4} l_i = k$$
$$0 < |\gamma| \leqslant 1 \tag{23}$$
$$0 < Q \leqslant 1$$

where $i = 1, 2, 3, 4$; the $l_{i\text{-min}}$ and $l_{i\text{-max}}$ are the minimum and maximum lengths of the $i$th pole, respectively; the constraint $\sum_{i=1}^{4} l_i$ means that the sum of the four rod lengths is unchanged.

The assembled free-tail based tail-sitter VTOL is shown in Fig.13.



Fig.13    Tail-sitter VTOL UAV incorporating free-tail bionic technology

The landing gear of the tail-sitter VTOL UAV is comprised of a single leg with a mass of 1 kg, is capable of efficiently supporting a mass exceeding 5 kg.

## 4    Tail-Sitter VTOL UAV Landing Test

To confirm the landing stability and safeguard the structural integrity of the aircraft during the initial development phase, a series of drop tests are conducted under varying working conditions. These tests are carried out using the drop test bench, which is illustrated in Fig.14.
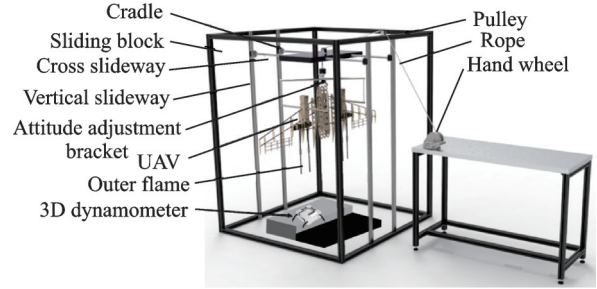


(a) Structure of tail-sitter VTOL UAV drop test bench



(b) Prototype of tail-sitter VTOL UAV drop test bench

Fig.14    Tail-sitter VTOL UAV drop test bench

The primary componentry of the testing apparatus comprises of a profile outer frame, a vertical guide rail, a hanging basket, and a force measuring platform. The prototype is securely fastened to the hanging basket via a connecting rod interposed with the vector surface. The hanging basket, which uses bearings to slide along the vertical guide rail, can adjust the drop height via the retraction of its rope, thereby simulating vertical landing motions. Moreover, the adjustable cross height structure of the hanging basket enables the attitude control of the prototype.

Through the drop shock test, as depicted in Fig.15, the tail-sitter VTOL UAV demonstrates adaptive landing capabilities across various attitudes, even in scenarios with ground inclinations exceeding 20°. The stability during these maneuvers surpassed that of traditional rigid landing gear, as evidenced by the observations presented in Figs.16—18.

Fig.15    Landing test of tail-sitter VTOL UAV landing gear
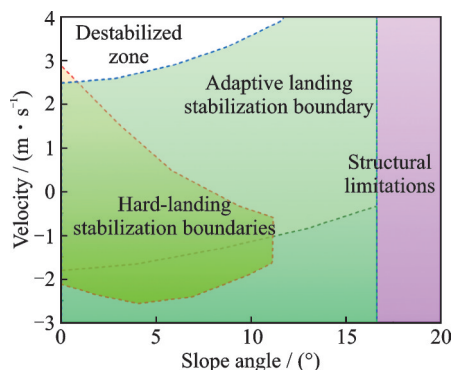


Fig.16    Landing stability boundary
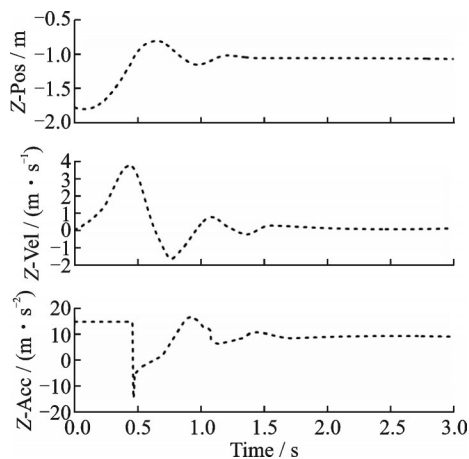


Fig.17    Fuselage center of gravity position and orientation for landing



(a) Center of gravity position



(b) Center of gravity orientation
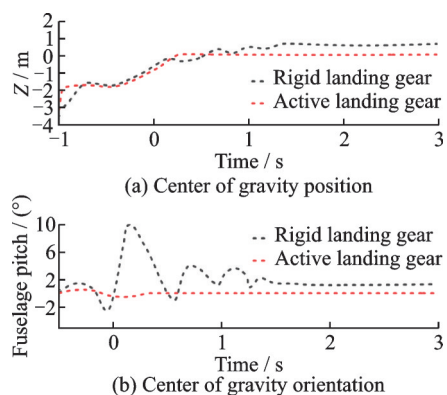
Fig.18    Fuselage center of gravity position and orientation for slope landing

The landing loads of the tail-sitter VTOL UAV, as depicted in Figs.19—21, are acquired through the employment of sensors located at the landing gear joints of the tail-sitter and the utilization of bottom force gauges. These measurements exhib-
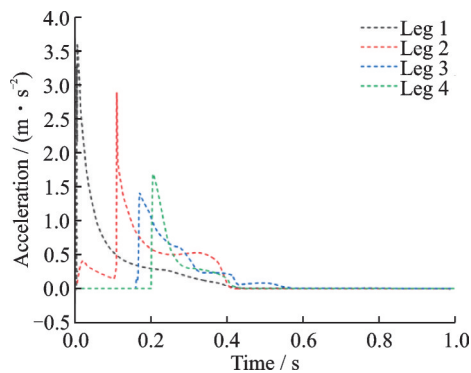


Fig.19    Acceleration of each landing leg of landing gear
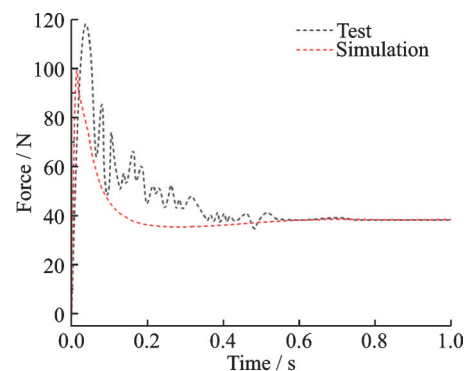


(a) Left first touchdown landing gear
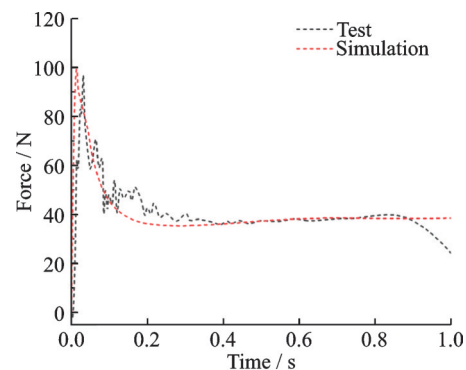


(b) Left last touchdown landing gear
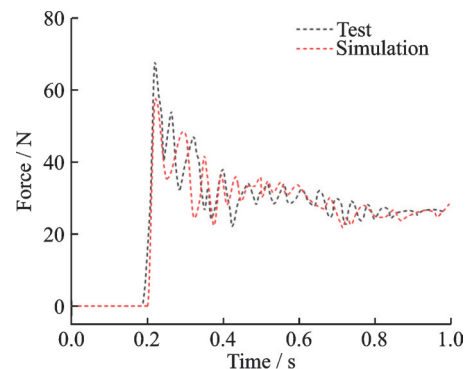


(c) Right first touchdown landing gear
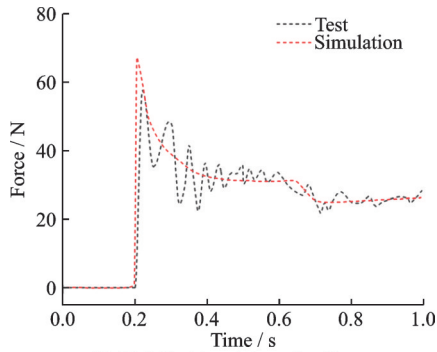
(d) Right last touchdown landing gear

Fig.20    Landing load of each landing gear
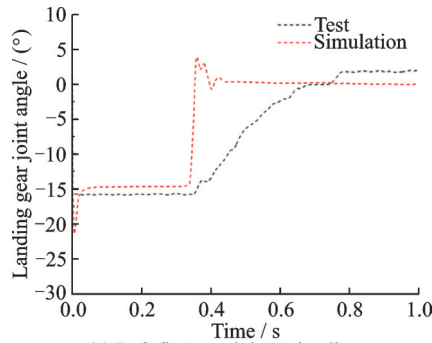

(a) Left first touchdown landing gear
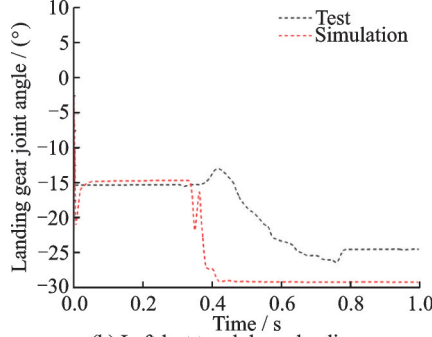

(b) Left last touchdown landing gear
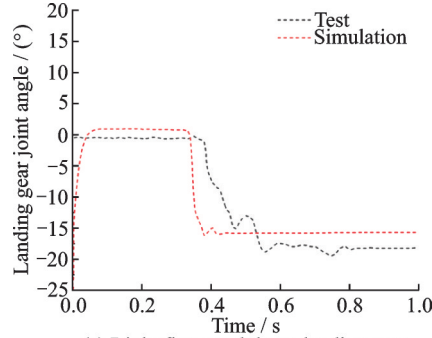

(c) Right first touchdown landing gear
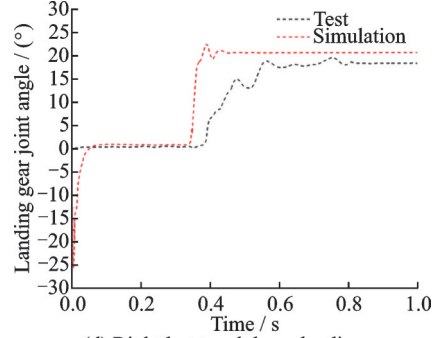

(d) Right last touchdown landing gear

Fig.21    Landing gear joint angles

it a significant resemblance to the landing dynamics of a cat，as simulated in the aforementioned study.

## 5    Conclusions

This study presents a technical solution for the tail-sitter VTOL UAV，which incorporates the use of a takeoff / landing device that optimizes the overall layout.

（1）The landing gear control is simplified by adopting the virtual center of mass force system allocation，utilizing a neural network to train the inner and outer double loops of the landing gear control based on a single point dataset of the cat centroid. This optimization results in a dynamically smoothed trajectory for the landing gear of a tail-sitter VTOL UAV under mode mutation. Although the biological structure of a cat has excellent landing performance，its large number of nodes necessitates extremely demanding data reconstruction accuracy for data classification，pattern recognition，and other scenarios. The optimized landing response speed is improved by 2/3 compared to the traditional PID control，and the maximum landing speed is reduced by 40%.

（2）The landing gear has been designed with a focus on structural and functional integration，allowing seamless adaptation to both vertical and horizontal flight modes. This innovative solution resolves the conflict between maintaining the height of the tail wing and the fuselage while enabling the landing gear to retract and extend in line with the overall shape of the aircraft. The landing gear length of the free-tail affects aerodynamic efficiency and landing stability. Therefore，it is necessary to retransform the similarity of the landing process after multi-objective optimization of the landing gear ratio. The optimized tail-sitter VTOL UAV incorporating free-tail bionic technology has improved landing stability，particularly compared to traditional fixed landing gear. Drop shock tests support this，demonstrating greater improvement in terrain adaptability and stabilization speed. In the future，the study hopes to optimize the takeoff and landing performance of tail-sitter VTOL UAV with the help of more other biomechanics.

## References

[1]　ALWATEER M, LOKE S W. Emerging drone services: Challenges and societal issues[J]. IEEE Technology and Society Magazine, 2020, 39(3): 47-51.

[2]　KUBO D, SUZUKI S. Tail-sitter vertical takeoff and landing UAV: Transitional flight analysis[J]. Journal of Aircraft, 2012, 45(1): 292-297.

[3]　DE WAGTER C, RUIJSINK R, SMEUR E J J, et al. Design, control, and visual navigation of the delftacopter VTOL tail-sitter UAV[J]. Journal of Field Robotics, 2018, 35(6): 937-960.

[4]　TANG Wei, SONG Bifeng. Transitional flight equilibrium and performance study for the X-NMRL tail-sitter VTOL MAV[J]. Proceedings of the Institution of Mechanical Engineers: Part G Journal of Aerospace Engineering, 2019, 233(8): 3056-3077.

[5]　WANG K, KE Y, CHEN B M. Autonomous reconfigurable hybrid tail-sitter UAV U-Lion[J]. Science China Information Sciences, 2017(3): 1-16.

[6]　BAE J, LEE J, JANG A, et al. Smart sky eye system for preliminary structural safety assessment of buildings using unmanned aerial vehicles[J]. Sensors, 2022, 22(7): 2762-2778.

[7]　KUANG Minchi, ZHU Jihong, WANG Wufan, et al. Flight controller design and demonstration of a thrust-vectored tailsitter[C]//Proceedings of 2017 IEEE International Conference on Robotics and Automation. Singapore: IEEE, 2017: 5169-5174.

[8]　ZOU Xu, LIU Zhenbao, ZHAO Wen, et al. Design and implementation of a hardware-in-the-loop simulation platform for a tail-sitter UAV[J]. Aircraft Engineering and Aerospace Technology, 2023, 95(6): 985-994.

[9]　RAMÍREZ-PÉREZ J, MELO-BARRERA F, AYALA-BOBADILLA L. Age and growth of pacific golden-eye tilefish (caulolatilus affinis) in the central region of the gulf of california[J]. Ciencias Marinas, 2011, 37(1): 71-85.

[10]　RODERICK W R T, CUTKOSKY M R, LENTINK D. Bird-inspired dynamic grasping and perching in arboreal environments[J]. Science Robotics, 2021, 6(61): 7562-7577.

[11]　KUANG Minchi, ZHU Jihong, WU Degui. Tail-sitter vertical takeoff and landing control for thrust-vectored unmanned aerial vehicle[J]. Control Theory & Applications, 2015, 32(11): 1449-1456.

[12]　DI LEO C V, LEÓN B, WACHLIN J, et al. Design of a crashworthy cable-driven four-bar link robotic landing gear system[J]. Journal of Aircraft, 2020, 57(2): 224-244.

[13]　MANIVANNAN V, LANGLEY J P, COSTELLO M, et al. Rotorcraft slope landings with articulated landing gear[C]//Proceedings of AIAA Atmospheric Flight Mechanics (AFM) Conference. Boston, MA: AIAA, 2013: 1338-1354.

[14]　RODERICK W R T, CUTKOSKY M R, LENTINK D. Bird-inspired dynamic grasping and perching in arboreal environments[J]. Science Robotics, 2021. DOI:10.1126/scirobotics.abj7562.

[15]　ERBIL M A, PRIOR S D, KEANE A J. Design optimisation of a reconfigurable perching element for vertical takeoff / landing unmanned aerial vehicles[J]. International Journal of Micro Air Vehicles, 2013, 5(3): 207-228.

[16]　ANG K, CUI J Q, PANG T, et al. Design and implementation of a thrust-vectored unmanned tail-sitter with reconfigurable wings[J]. Unmanned Systems, 2015, 3(2): 143-162.

[17]　HUANG T, ELIBOL A, CHONG N Y. Enabling landings on irregular surfaces for unmanned aerial vehicles via a novel robotic landing gear[J]. Intelligent Service Robotics, 2022, 15(2): 231-243.

[18]　ZHONG Jingyang, WANG Chen. Transition characteristics for a small tail-sitter unmanned aerial vehicle[J]. Chinese Journal of Aeronautics, 2021, 34(10): 220-236.

[19]　ASLAN S, OKTAY T. Path planning of an unmanned combat aerial vehicle with an extended-treatment-approach-based immune plasma algorithm[J]. Aerospace, 2023, 10(5): 487.

[20]　KOSE O, OKTAY T. Simultaneous design of morphing hexarotor and autopilot system by using deep neural network and SPSA[J]. Aircraft Engineering and Aerospace Technology, 2023, 95(6): 939-949.

[21]　ÇOBAN S. Autonomous performance maximization of research-based hybrid unmanned aerial vehicle[J]. Aircraft Engineering and Aerospace Technology, 2020, 92(4): 645-651.

[22]　IANUZZI A, PICKAR J G, KHALSA P S. Determination of torque-limits for human and cat lumbar spine specimens during displacement-controlled physiological motions[J]. The Spine Journal, 2009, 9(1): 77-86.

[23]　LI Jianfeng, ZHOU Yu, DONG Mingjie, et al. Isokinetic muscle strength training strategy of an ankle rehabilitation robot based on adaptive gain and cascade PID control[J]. IEEE Transactions on Cognitive and Developmental Systems, 2023, 15(1): 100-110.

**Authors**  Mr. **QI Hao** has been pursuing his Ph.D. degree in aircraft design at Nanjing University of Aeronautics and Astronautics (NUAA) since 2020. His research interests include innovative takeoff and landing technologies and system dynamics of vertical takeoff and landing vehicles, and he has published more than 10 academic papers and authorized 15 national invention patents.

Prof. **WEI Xiaohui** graduated from NUAA in 2006 with a Ph.D. degree in vehicle design, and he has been working in NUAA since 2006. His research interests include intelligent vehicle systems. He is currently a professor, doctoral director, dean of the School of Aeronautics, and the director of the Helicopter Research Institute of NUAA.

**Author contributions**  Prof. **WEI Xiaohui** designed the study, Mr. **LI Qingyang** complied the models, Mr. **WU Jiayue** conceived and designed the experiments, Mr. **QI Hao** interpreted the results and wrote the manuscript. Dr. **PENG Yiming** contributed to data for the analysis. Prof. **NIE Hong** contributed to the discussion and background of the study. All authors commented on the manuscript draft and approved the submission.

**Competing interests**  The authors declare no competing interests.

（Production Editors：XU Chengting，WANG Jie）

# 基于仿生技术的尾座式 **VTOL** 无人机起降稳定控制及轨迹优化

齐　浩[1,2]，李青洋[1,3]，吴嘉越[1,4]，彭一明[1,2]，聂　宏[1,2]，魏小辉[1,2]

（1.南京航空航天大学航空航天结构力学及控制全国重点实验室，南京 210016，中国；2.南京航空航天大学飞行器先进设计技术国防重点学科实验室，南京 210016，中国；3.中国航空动力机械研究所，株洲 412002，中国；4.北京航空航天大学自动化科学与电气工程学院，北京 100191，中国）

**摘要**：尾座式垂直起降（Vertical takeoff / landing，VTOL）无人机（Unmanned aerial vehicle，UAV）稳定性差，与传统起落架的适配性低。针对上述问题，提出了一种采用自由尾翼技术的新型起落架。该起落架采用串联多级结构，在降低机身高度的同时，保证了巡航状态下尾翼力臂的长度，并通过虚拟中心点力分布技术对动态着陆过程进行调控，简化了控制过程，有利于模式转换过程中的无缝轨迹优化。随后基于猫中心点单点数据集，利用神经网络对起落架控制进行训练，有效提高了起落架自适应起落速度和精度。最后，结合无人机不同模式的参数要求，进行多目标优化和相似性转换，有效提高了尾座式垂直起降无人机的着陆适应性和稳定性。

**关键词**：无人机；垂直起降；起飞/着陆技术；稳定性控制；仿生技术